



# Bayesian probabilistic assessment of occupant comfort of high-rise structures based on structural health monitoring data

Y.W. Wang<sup>a,b</sup>, C. Zhang<sup>a,b</sup>, Y.Q. Ni<sup>a,b,\*</sup>, X.Y. Xu<sup>a,b</sup>

<sup>a</sup> Department of Civil and Environmental Engineering, The Hong Kong Polytechnic University, Hung Hom, Kowloon, Hong Kong, China

<sup>b</sup> Hong Kong Branch of Chinese National Engineering Research Center on Rail Transit Electrification and Automation, Hung Hom, Kowloon, Hong Kong, China

## ARTICLE INFO

Communicated by Spilios Fassois

### Keywords:

High-rise structures  
Tropical cyclones  
Occupant comfort  
Structural health monitoring  
Bayesian inference

## ABSTRACT

Comfort performance of high-rise structures during strong winds is significant to inhabitants. Despite the significance, procedures for evaluating occupant comfort in serviceability limit states have not been as well developed as those for strength-based design of high-rise structures. One of the difficulties arises from uncertainties associated with the parameters in occupant comfort assessment, which pertain to the acceleration response magnitude and its relationship to human reaction to the motion. The comfort assessment is in general conducted by examining whether the wind-induced acceleration response satisfies some occupant comfort criteria. Such a deterministic approach, however, fails to account for uncertainty inherent in the wind-induced acceleration response as it is affected by the wind field of stochastic nature and uncertainty about the aerodynamic loads and the structure's dynamic behavior. In view of this, a Bayesian probabilistic approach is proposed in this study to evaluate the occupant comfort of high-rise structures. First, a Bayesian regression model is formulated for characterizing wind-induced acceleration responses of a structure by use of structural health monitoring (SHM) data acquired during strong winds, thereby enabling to account for the uncertainty contained in the monitored acceleration responses and quantify the uncertainty in modeling and prediction. Based on the predicted acceleration distribution and reliability theory, a safety index is then elicited to perform probabilistic assessment of occupant comfort in wind-induced motion of the structure. In the case study, field monitoring data acquired from a supertall structure of 600 m high during six tropical cyclones are used to illustrate the proposed approach, including the evaluation of occupant comfort of the structure under extreme wind speeds.

## 1. Introduction

The use of high strength materials and advanced structural systems makes the modern tall buildings to be higher and more flexible, enabling the possibility of buildings soaring to the height of 1000 m [1]. As a result, such supertall structures are susceptible to wind-induced vibration. It has been reported that high-rise structures in coastal cities became unserviceable when suffering from excessive wind-induced motion during windstorms. Prolonged exposure to these vibrations may cause occupant discomfort, triggering emotional and physical reactions such as concern, anxiety, fear, dizziness, and headaches [2,3]. In Hong Kong, the typhoon Mangkhut

\* Corresponding author at: Department of Civil and Environmental Engineering, The Hong Kong Polytechnic University, Hung Hom, Kowloon, Hong Kong, China.

E-mail address: [ceyqni@polyu.edu.hk](mailto:ceyqni@polyu.edu.hk) (Y.Q. Ni).

<https://doi.org/10.1016/j.ymssp.2021.108147>

Received 13 December 2020; Received in revised form 17 April 2021; Accepted 12 June 2021

Available online 23 June 2021

0888-3270/© 2021 The Author(s). Published by Elsevier Ltd. This is an open access article under the CC BY-NC-ND license

(<http://creativecommons.org/licenses/by-nc-nd/4.0/>).

in 2018 with a record-breaking strength and devastating damage is a live example. High winds caused some high-rise buildings to sway violently, and shattered windows of others. Many habitants residing in higher building stories felt uncomfortable and even scared due to excessive vibration [4]. These facts evidence again that occupant comfort is a crucial issue in the design of high-rise structures.

Occupant comfort during wind-induced motion of high-rise structures can be assessed by means of dynamic response indicators such as acceleration, velocity and displacement [5]. Among them, acceleration is unanimously recognized as the one most intimately related to the occupant comfort [6,7]. With the purpose of better understanding this relationship, a number of studies have been pursued over the years, including simulations and experimental tests, field measurements of real structures, and survey via questionnaires to habitants [8–10]. In the current design of modern tall buildings, wind tunnel tests are routinely employed to determine the wind-induced top floor acceleration [11] so that occupant comfort can be assessed against some occupant comfort criteria such as ISO 6897 [12], ISO 10,137 [13], and AIJ Guidelines [14]. When the wind tunnel test results reveal that the wind-induced acceleration exceeds the occupant comfort limit states, certain mitigation measures such as increase of structural damping by installing vibration control devices and/or amendment of structural system or building aerodynamic shape are usually suggested.

While wind tunnel test is widely used in the design stage of tall buildings, full-scale measurements under real wind conditions are viewed as the most reliable method for evaluating the wind-induced vibration and occupant comfort of built tall buildings [15]. The first report of field investigation was the landmark study conducted by Hansen et al. [16], where the occupants of two tall office buildings (167 m high) were surveyed after a wind-attack event and questioned concerning “how many times a year a similar experience would occur before it become objectionable?”. By performing so, the investigators gained a sense of the relationship between the motion intensity and the percentage of people objecting to the building vibration. Later on, more field tests of wind-induced vibration and surveys of the residents were conducted on high-rise structures during wind storms [9,17–20]. One of the longest ongoing and perhaps most monumental studies is the Chicago full-scale monitoring program [9]. The program was established in 2001 to correlate the in-situ full-scale measured response characteristics of tall buildings, with computer-based analytical and wind tunnel models for the advancement of state-of-the-art design of tall buildings. Over the recent decades, full-scale measurements of both wind effects on and the ensuing dynamic characteristics of supertall structures (greater than 300 m in height) have been increasingly executed, and the results of which were highly valuable to the professionals involved in designing such buildings. For example, structural health monitoring (SHM) system has been implemented on the world’s tallest building, Burj Khalifa of 828 m high, for wind and structural response monitoring [21]. Also, wind effects on over 10 supertall structures in China during tropical cyclones have been comprehensively evaluated through deploying long-term or short-term SHM systems [22–28].

With progressively cumulated SHM data, numerous researchers have attempted to establish correlation regularity between the wind-induced RMS/peak acceleration of high-rise structures and the mean wind speed [22,23,25,29,30]. However, the correlation models were mostly obtained in a deterministic manner. With such formulated models, maximum acceleration response can be predicted and compared with the comfort criteria for occupant comfort assessment. One major drawback is that the accuracy of model parameter estimation is affected by the valid data volume. Limited incomplete data would lead to inaccurate parameter estimation. More importantly, the formulated models fail to account for the uncertainty inherent in the monitoring data and interpret the model error. In fact, the RMS/peak acceleration response is affected by the wind field of stochastic nature and by epistemic uncertainties on the structure’s aerodynamic behavior and its structural properties [6]. It is therefore particularly essential to characterize these uncertainties in the assessment of structural dynamic response and occupant comfort. The effects of these uncertainties in the serviceability design of buildings have been addressed by different ways [3,6,31,32], but all in the conventional (frequentist) probabilistic context rather than the Bayesian probabilistic context.

This study aims to develop a Bayesian probabilistic framework for occupant comfort evaluation of high-rise structures using SHM data. The Bayesian probabilistic approach offers two appealing merits: (i) the model parameters in Bayesian context are treated as random variables rather than deterministic quantities and thus are able to accommodate uncertainty contained in the monitoring data, and (ii) the formulated model enables the quantification of model error and prediction uncertainty. In this connection, a Bayesian methodology will first be developed for probabilistic modeling of the nonlinear relationship between the acceleration response and wind speed as well as for probabilistic assessment of the occupant comfort in serviceability limit states. Long-term monitoring data of wind velocity and acceleration response recorded by an SHM system deployed on the 600 m high Canton Tower during 6 tropical cyclones between 2011 and 2013 will then be utilized to verify the proposed methodology. This paper is structured as follows. Section 1 briefly reviews the state-of-the-art research in relation to occupant comfort assessment of high-rise structures. In Section 2, a Bayesian wind-acceleration-relation (WAR) model characterizing the wind-induced structural response is formulated. Section 3 introduces the instrumented supertall structure, the SHM system, and the monitoring data collected during 6 tropical cyclones. In Section 4, the occupant comfort of the supertall structure in serviceability limit states is evaluated. Conclusions are drawn in Section 5.

## 2. Bayesian approach for wind-induced response modeling

### 2.1. Bayesian WAR model

The previous field measurements of wind effects on high-rise structures have revealed that there exists a power function relationship between the acceleration response and mean wind speed [22,23,25,29,30], which can be expressed as

$$Acc_i = a_1 \bar{U}_i^{b_1}, \quad i = 1, 2, \dots, n \quad (1)$$

where  $Acc_i$  represents the root mean square (RMS) or peak acceleration at the  $i$ th time interval (e.g., 10 min for each interval);  $\bar{U}_i$  is the

corresponding mean wind speed;  $a_1$  and  $b_1$  are unknown parameters; and  $n$  denotes the total number of time intervals in consideration. Taking the logarithm of both sides of Eq. (1), we obtain

$$\log Acc_i = \log a_1 + b_1 \log \bar{U}_i, \quad i = 1, 2, \dots, n \tag{2}$$

By defining  $y_i = \log Acc_i$ ,  $x_i = \log \bar{U}_i$ ,  $\beta_1 = \log a_1$  and  $\beta_2 = b_1$ , the above log-transformed power function becomes the following linear function

$$y_i = \beta_1 + \beta_2 x_i, \quad i = 1, 2, \dots, n \tag{3}$$

In the Bayesian context, the linear regression model of the relationship between the response variables  $y_i$  and explanatory variables  $x_i$  can be expressed in matrix form as [33–35]

$$Y = X\beta + \varepsilon, \quad \varepsilon \sim N(0, \sigma^2 I) \tag{4}$$

with

$$Y = \begin{bmatrix} y_1 \\ y_2 \\ \vdots \\ y_n \end{bmatrix}, \quad \beta = \begin{bmatrix} \beta_1 \\ \beta_2 \end{bmatrix}, \quad X = \begin{bmatrix} 1 & x_1 \\ 1 & x_2 \\ \vdots & \vdots \\ 1 & x_n \end{bmatrix}, \quad \varepsilon = \begin{bmatrix} \varepsilon_1 \\ \varepsilon_2 \\ \vdots \\ \varepsilon_n \end{bmatrix}$$

where the error  $\varepsilon$  is a normally distributed random variables with zero mean and variance  $\sigma^2$ ;  $I$  represents the unit matrix of dimension  $n$ . The density form of Eq. (4) can be expressed as

$$f(Y|X, \beta, \sigma^2) = \frac{1}{(2\pi\sigma^2)^{n/2}} \exp\left[-\frac{(Y - X\beta)^T(Y - X\beta)}{2\sigma^2}\right] \tag{5}$$

where the coefficient vector  $\beta$  and the regression variance  $\sigma^2$  are unknown parameters to be estimated. In pursuit of Bayesian inference, a prior distribution should be specified for  $\beta$  and  $\sigma^2$ . A popular choice of the prior distribution is conjugate normal inverse gamma, that is, normal distribution for  $\beta$  and inverse gamma distribution for  $\sigma^2$ . As the variance  $\sigma^2$  is non-negative, the inverse gamma distribution describing a continuous probability distribution on the positive real abscissa is perfectly suitable for the variance [36,37]. Its prior distribution can be expressed as

$$f(\beta, \sigma^2) = f(\beta|\sigma^2)f(\sigma^2) \tag{6}$$

with

$$f(\beta|\sigma^2) = N\left(\beta_0, \sigma^2 \Sigma_0\right) = \frac{1}{(2\pi\sigma^2)^{k/2} |\Sigma_0|^{1/2}} \exp\left[-\frac{(\beta - \beta_0)^T \Sigma_0^{-1} (\beta - \beta_0)}{2\sigma^2}\right]$$

$$f(\sigma^2) = IG\left(\frac{a}{2}, \frac{b}{2}\right) = \frac{\left(\frac{b}{2}\right)^{a/2}}{\Gamma\left(\frac{a}{2}\right)} (\sigma^2)^{-a/2-1} \exp\left(-\frac{b}{2\sigma^2}\right)$$

where the coefficients  $\beta_0$ ,  $\Sigma_0$ ,  $a$  and  $b$  can be determined based on the prior information stemming from an earlier data analysis, the expert knowledge, or the published literature.

According to Bayes' theorem, the posterior distribution  $f(\beta, \sigma^2|Y, X)$  is proportional to the likelihood function  $f(Y|X, \beta, \sigma^2)$  multiplied by the prior distribution  $f(\beta, \sigma^2)$  [38]

$$\begin{aligned} f(\beta, \sigma^2|Y, X) &\propto f(Y|X, \beta, \sigma^2) \times f(\beta, \sigma^2) \\ &\propto (\sigma^2)^{-n/2} \exp\left[-\frac{(Y - X\beta)^T(Y - X\beta)}{2\sigma^2}\right] \\ &\times (\sigma^2)^{-k/2} \exp\left[-\frac{(\beta - \beta_0)^T \Sigma_0^{-1} (\beta - \beta_0)}{2\sigma^2}\right] \\ &\times (\sigma^2)^{-a/2-1} \exp\left(-\frac{b}{2\sigma^2}\right) \end{aligned} \tag{7}$$

Combining the density functions and the joint posterior yields

$$f(\beta, \sigma^2 | Y, X) \propto (\sigma^2)^{-k/2} \exp \left\{ -\frac{1}{2\sigma^2} \left( \beta^T \left[ X^T X + \sum_0^{-1} \right] \beta - 2\beta^T \left[ X^T Y + \sum_0^{-1} \beta_0 \right] + Y^T Y + \beta_0^T \sum_0^{-1} \beta_0 \right) \right\} \times (\sigma^2)^{-(a+n)/2-1} \exp \left( -\frac{b}{2\sigma^2} \right) \tag{8}$$

It is found that Eq. (8) is again a kernel normal inverse gamma distribution, factored as the conditional posterior distribution of  $\beta$  multiplied by the marginal posterior distribution of  $\sigma^2$

$$f(\beta, \sigma^2 | Y, X) = f(\beta | \sigma^2, Y, X) \times f(\sigma^2 | Y) \tag{9}$$

where

$$f(\beta | \sigma^2, Y, X) \sim N(\beta^*, \sigma^2 \sum^*) \tag{10}$$

$$f(\sigma^2 | Y) \sim IG\left(\frac{a^*}{2}, \frac{b^*}{2}\right) \tag{11}$$

with

$$\beta^* = \left( X^T X + \sum_0^{-1} \right)^{-1} \left( X^T Y + \sum_0^{-1} \beta_0 \right), \quad \sum^* = \left( X^T X + \sum_0^{-1} \right)^{-1}$$

$$a^* = a + n, \quad b^* = b + Y^T Y + \beta_0^T \sum_0^{-1} \beta_0 - \beta^{*T} \sum^* \beta^*$$

### 2.2. Gibbs sampler for parameter estimation

With the assumption of natural conjugate prior, the analytical expression of joint posterior distribution for the unknown parameters has been elicited in the previous section. However, the marginal posterior distributions of  $\beta$  and  $\sigma^2$  are what we are concerned about. In practice, it is intractable to get the marginal posterior distributions by integrating  $\sigma^2$  and  $\beta$  out of the joint posterior distribution, so we use Markov chain Monte Carlo (MCMC) sampling methods to draw samples from the posterior in order to approximate the marginal posterior distributions. As one of MCMC methods, Gibbs sampler has been widely used since its advent in 1990 [39]. It is favorable for scenarios where sampling from a multivariate posterior is infeasible, but rather sampling from the conditional distributions for each variable is feasible. The idea behind the Gibbs sampler is to generate a sample from the distribution of each variable in turn, conditional on the current values of other variables. It is provable that the sample sequences constitute a Markov chain, and the stationary distribution of the Markov chain is just the sought-after posterior distribution of the variable addressed. The iterative process of Gibbs sampler is as follows [38]:

- (1) Initialize the parameter values  $\{\beta^{(0)}, \sigma^{2(0)}\}$  and set  $k = 1$ ;
- (2) Sample  $\beta^{(k)}$  from the conditional distribution  $f(\beta | Y, X, \sigma^{2(k-1)})$  (Eq. (10));
- (3) Sample  $\sigma^{2(k)}$  from the conditional distribution  $f(\sigma^2 | Y, \beta^{(k)})$  (Eq. (11));
- (4) Let  $k = k + 1$ , go back to (2) and (3) and repeat until  $L$  samples

$\{\beta^{(k)}, \sigma^{2(k)}; k = 1, \dots, L\}$  are obtained.

After sufficient iterations, the samples generated from the Gibbs sampler can be viewed as the samples of the marginal distribution. Thus, discarding the preceding part of the samples, the remainder (after convergence) can be used for Bayesian inference. The simplest way to determine convergence of the Markov chain is visual inspection, that is, by checking the trend of the trace plot. If a Markov chain has converged to its distribution, the trace plot will fluctuate smoothly without any trend. Otherwise, a trend will appear. Care must also be taken as to whether the Markov chain converges to a local solution. A more rational approach is based on the convergence diagnostic (CD) test statistic proposed by Geweke [40], which measures the equality of both the means of the first and last parts of a Markov chain. Involved is a division of a total of  $L$  draws from the Gibbs sampler into initial  $L_0$  draws discarded as burn-in replications, and the remaining  $L_1$  draws. Further, the latter is divided into three sets: a first set of  $L_A$  draws, a middle set of  $L_B$  draws and a final set of  $L_C$  draws. It has been shown that the setting of  $L_A = 0.1L_1, L_B = 0.5L_1, L_C = 0.4L_1$  works well in practice [41]. For the purpose of calculating the convergence diagnostic, the middle set of draws is discarded for making it likely that the first and last sets of draws are independent of each other. Let  $M_{L_A}$  and  $M_{L_C}$  be the averages of the first and last sets of draws, and  $\sigma_{L_A}$  and  $\sigma_{L_C}$  be the standard errors of these two parts, the test statistic is then obtained by

$$CD = \frac{M_{L_A} - M_{L_C}}{\sqrt{\frac{\sigma_{L_A}^2}{L_A} + \frac{\sigma_{L_C}^2}{L_C}}} \tag{12}$$

which is an asymptotic standard normal distribution as  $N(0,1)$ . Large  $CD$  value implies a significant difference between the first and last sets of draws, and in such situation the number of total Gibbs iterations should be increased to generate more samples. If the convergence diagnostic indicates that enough draws have been obtained, then final results can be calculated based on the complete set of the remaining  $L_1$  draws.

### 3. Instrumentation and monitoring during tropical cyclones

#### 3.1. Instrumented structure

The Canton Tower located in the city of Guangzhou, China, is a supertall structure with a total height of 600 m. It includes a main tower and a mast above. The main tower is 454 m high and comprises an interior reinforced concrete (RC) column structure surrounded by an exterior latticed steel frame with helical shape. The interior column has a constant ellipse cross-section of  $14\text{ m} \times 17\text{ m}$ , while the geometric configuration of the exterior frame varies with height, which decreases from  $50\text{ m} \times 80\text{ m}$  at the ground level to the minimum of  $20.7\text{ m} \times 27.7\text{ m}$  at the height of 280 m (waist level), and then increases to  $41\text{ m} \times 55\text{ m}$  at the very top of the main tower (454 m). There are 37 unevenly distributed floors connecting the interior RC column and exterior steel frame that serve for various sightseeing and tourism functions including observatory decks, revolving restaurants, exhibition spaces, conference rooms, etc. The mast reaching 146 m high above the tower top is a latticed steel structure with an octagonal cross-section of 14 m in the maximum diagonal.

A sophisticated long-term SHM system consisting of over 700 sensors has been implemented on the Canton Tower by The Hong Kong Polytechnic University [42–44]. Only the sensors in relation to this study are described herein. As part of the SHM system, a total of twenty uniaxial accelerometers of Model AS-2000C (Tokyo Sokushin Co. Ltd., Tokyo, Japan) were installed at eight levels of the interior RC column at the heights of 30.6 m, 119.3 m, 171.1 m, 228.5 m, 275.3 m, 332.2 m, 384.2 m and 446.8 m, as shown in Fig. 1a. The 4th and 8th levels were equipped with four uniaxial accelerometers, two along the short-axis of the RC column and the other two along the long-axis. On the other six levels, each cross-section was equipped with two uniaxial accelerometers, one along the short-axis of the RC column and the other along the long-axis (Fig. 1c and 1d). One propeller anemometer of Model 05103L (R. M. Young Company, Traverse City, Michigan, USA) was deployed at the top of the main tower, which is 461 m above the ground (Fig. 1b). The data acquired by the accelerometers and anemometer were recorded synchronously using a data acquisition unit at a sampling rate of 50 Hz. The specifications of the accelerometers and anemometer are given in Table 1.

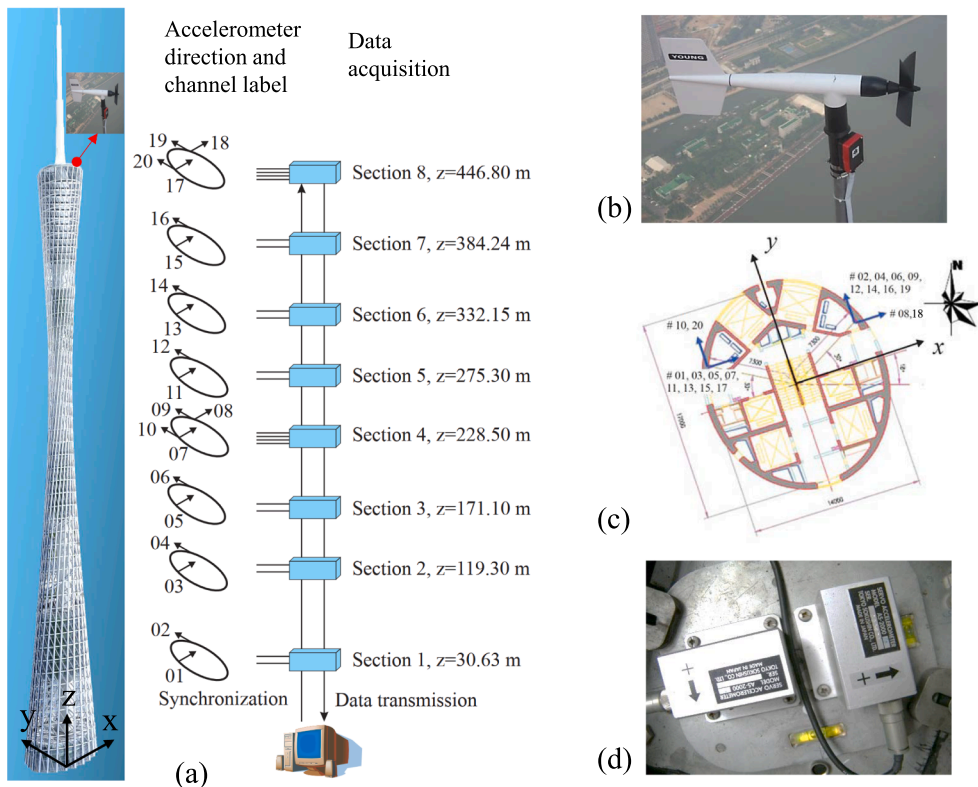


Fig. 1. (a) Deployment of accelerometers, anemometer and data acquisition system; (b) Anemometer; (c) Layout of accelerometers in cross-section plane; (d) Accelerometers.

### 3.2. Acceleration responses collected during tropical cyclones

This study uses the field monitoring data collected by the SHM system during 6 tropical cyclone events between 2011 and 2013, that imposed intense structural vibrations of the Canton Tower. The basic information about these tropical cyclones is listed in Table 2. The total time duration of the extracted data during the 6 tropical cyclones attacking the city is about 11,210 min (186.8 h). According to the Hong Kong Observation (HKO), the threat or the effect of a tropical cyclone is indicated by a set of tropical cyclone warning signals. The warning signal No. 10 indicates that the winds near sea level reach a sustained speed exceeding 118 km/h (33.8 m/s), while the warning signals No. 8 and No. 3 indicate that the winds near sea level reach sustained speeds of 63–117 km/h (17.5–32.5 m/s) and 41–62 km/h (11.4–17.2 m/s), respectively. Fig. 2 illustrates the time histories of 10-min mean wind speed and wind direction during the 6 tropical cyclones. It can be intuitively observed that most of the mean wind speeds are greater than 5 m/s, with the largest reaching nearly 30 m/s. The winds were blowing mostly from the southeast and southwest directions.

As the accelerations in both X and Y directions make significant contributions to the structural motions felt by habitants, it is reasonable to adopt the resultant acceleration [24]. The nondirectional RMS acceleration combining the two perpendicular motions is defined as

$$\delta_{acc} = \sqrt{\delta_{acc_x}^2 + \delta_{acc_y}^2} \tag{13}$$

where  $\delta_{acc}$  is the resultant RMS acceleration;  $\delta_{acc_x}$  and  $\delta_{acc_y}$  are the RMS accelerations in X and Y directions, respectively. Similarly, the resultant peak acceleration can be defined as [45]

$$P_{acc} = \varphi \times \sqrt{P_{acc_x}^2 + P_{acc_y}^2} \tag{14}$$

where  $P_{acc}$  is the resultant peak acceleration;  $P_{acc_x}$  and  $P_{acc_y}$  are the peak accelerations in X and Y directions, respectively;  $\varphi$  is a joint action factor which ranges between 0.7 and 1.0, and typically 0.8 to 0.9 [45]. The relationship between the RMS and peak accelerations can also be expressed as

$$P_{acc} = g_f \delta_{acc} = g_f \sqrt{\delta_{acc_x}^2 + \delta_{acc_y}^2} \tag{15}$$

where  $g_f$  is the gust factor, which can be estimated by the term  $\sqrt{2 \ln(fT)}$  ( $f$  is the fundamental frequency of the structure,  $T$  is the time interval in second) proposed by Melbourne and Palmer [46]. With the fundamental frequency  $f = 0.0928$  Hz for the Canton Tower and the time interval  $T = 10$  min = 600 s, the gust factor is estimated to be 2.83. In practice, the joint action factor can be indirectly estimated from the peak factor which is defined as  $\sqrt{P_{acc_x}^2 + P_{acc_y}^2} / \sqrt{\delta_{acc_x}^2 + \delta_{acc_y}^2}$ . The histogram of the peak factor values obtained from the measured acceleration responses in both X and Y directions is shown in the inserted panel of Fig. 3; it is seen that the majority of the peak factor values range from 2 to 5, with a mean of 3.28. Using this mean value of the peak factor, the joint action factor  $\varphi$  is estimated by equating Eqs. (14) with (15) to be approximately 0.85. Fig. 3 shows the time histories of the peak acceleration and the 10-min RMS acceleration. As expected, the variation tendencies of the peak and RMS accelerations during tropical cyclones are consistent roughly with the wind speed shown in Fig. 2(a).

## 4. Occupant comfort assessment

### 4.1. Formulation of Bayesian WAR models

As aforementioned, RMS and peak accelerations are appropriate indices for evaluating the occupant comfort of high-rise structures under wind actions. Hence, this study focuses on the RMS and peak acceleration responses under strong winds,

$$\delta_{acc} = a_1 \bar{U}^{b_1} \tag{16}$$

$$P_{acc} = a_2 \bar{U}^{b_2} \tag{17}$$

where  $\delta_{acc}$  and  $P_{acc}$  are the 10-min RMS and peak accelerations, respectively;  $\bar{U}$  is the 10-min mean wind speed;  $a_1$ ,  $b_1$ ,  $a_2$  and  $b_2$  are unknown parameters to be estimated. According to the Bayesian modeling methodology described in Section 2, Eqs. (16) and (17) are

**Table 1**  
Specifications of sensors.

Sensor	Measurand	Model	Specifications
Anemometer	Wind speed and direction	Model 05103L, R. M. Young Company, Traverse City, Michigan, USA	Rang: 0–100 m/s, 0–360°; Accuracy: wind speed ± 0.3 m/s, direction ± 3°
Accelerometer	Acceleration	Model AS-2000C, Tokyo Sokushin Co. Ltd., Tokyo, Japan	Rang: ±2 G; Accuracy: 1.225 V/G

**Table 2**  
Information about the 6 tropical cyclones (TC).

No.	Tropical cyclone	Date	Highest warning signal	Max 10-min mean wind speed (m/s)	Measurement duration ( $\times 10$ min)
TC1	Haima	23 June 2011	3	14.33	113
TC2	Nockten	29 July 2011	3	11.65	144
TC3	Nanmadol	31 Aug. 2011	3	10.16	144
TC4	Vicente	23–24 July 2012	10	28.75	288
TC5	Utor	14 Aug. 2013	8	14.26	144
TC6	Usagi	22–23 Sept. 2013	8	21.59	288

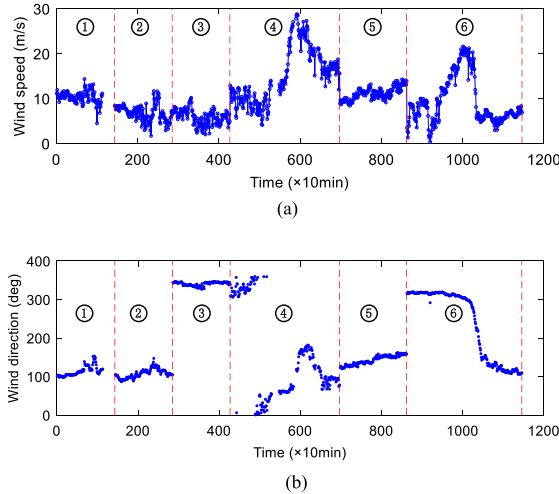


Fig. 2. Sequences of 10-min mean wind speed and direction: (a) Wind speed; (b) Wind direction.

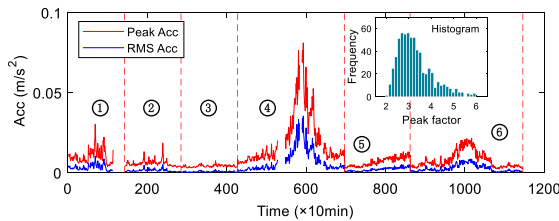


Fig. 3. Sequences of peak and RMS accelerations.

firstly transferred to linear regression models as Eq. (4). To implement the Bayesian regression analysis, a normal inverse gamma prior is adopted to depict the conjugate prior of the model parameters. Because of very little certainty of the parameters, we choose the prior distributions enabling to cover a wide range of the possible values. Here, we set  $\sum_0 = 100 \times I_2$  ( $I_2$  is two-dimensional unit matrix) and  $a = b = 0.001$ , which makes the prior distribution highly diffuse. In implementing the Gibbs sampler for estimation of the model parameters  $\beta_1$ ,  $\beta_2$  and  $\sigma^2$ , the total Markov chain iterations is chosen as 100,000, of which the first 50,000 ( $L_0 = 50,000$ ) iterations are discarded as burn-in replications. Thus, there remain 50,000 ( $L_1 = 50,000$ ,  $L_A = 0.1L_1$ ,  $L_B = 0.5L_1$ ,  $L_C = 0.4L_1$ ) posterior samples generated from the Gibbs sampler. In order to check if the posterior samples arise from a stationary distribution, both trace plots and CD test statistic are used to evaluate the convergence of the remaining posterior samples. As two Bayesian WAR models are formulated in terms of the peak and RMS accelerations, two sets of parameters are to be examined. Fig. 4 shows the sample paths and estimated posterior densities of the model parameters for RMS acceleration. Shown in the left panel are the sample paths of 50,000 remaining draws. By examining the trace plots, it is obvious that the Markov chain of posterior samples is stationary. The values of the CD listed in Table 3 are all close to zero, justifying that the retained samples meet the convergence criterion. The right panel in Fig. 4 shows the marginal posterior distributions of the model parameters ( $\beta_1$ ,  $\beta_2$  and  $\sigma^2$ ) and their fitting distributions, where normal and student-t distributions are applied to fit the distributions of  $\beta_1$  and  $\beta_2$ , and normal and inverse gamma distributions are used to fit the distribution of  $\sigma^2$ . Based on the maximum likelihood estimation for the goodness-of-fit tests, it is found that the performance of student-t distribution is better than normal distribution for fitting  $\beta_1$  and  $\beta_2$ , and inverse gamma distribution is more suitable for fitting  $\sigma^2$ . With the same prior distribution (conjugate normal inverse gamma) for model parameters, it is proven by analytic analysis that the marginal posterior distributions of  $\beta_1$  and  $\beta_2$  are of student-t distribution and the marginal posterior distribution of  $\sigma^2$  conforms to inverse

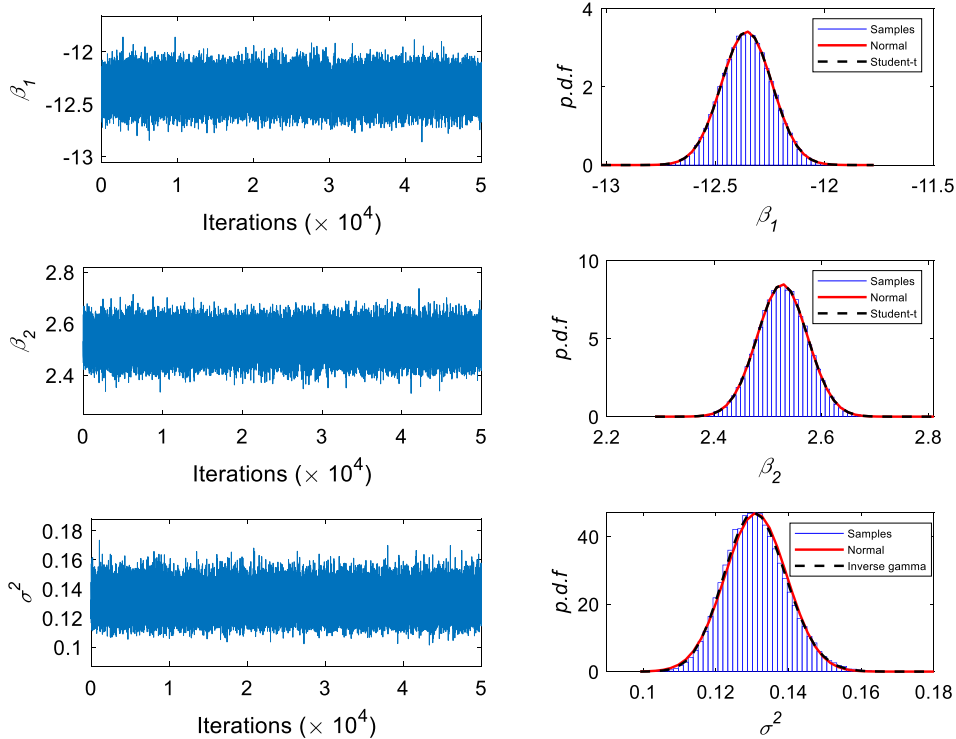


Fig. 4. Sample paths and estimated posterior densities for parameters (RMS acceleration).

Table 3  
Parameters of regression model in Eq. (4).

Model	Parameter	Mean	Standard deviation	95% confidence interval		CD
RMS	$\beta_1$	-12.357	0.116	-12.584	-12.132	0.001
	$\beta_2$	2.527	0.046	2.437	2.619	-0.001
	$\sigma^2$	0.131	0.008	0.115	0.149	-0.004
Peak	$\beta_1$	-11.829	0.105	-12.036	-11.623	0.000
	$\beta_2$	2.686	0.042	2.603	2.769	0.001
	$\sigma^2$	0.167	0.011	0.147	0.189	0.005

gamma distribution [47]. These findings are consistent with the theoretical solutions. More detailed parameter information, such as posterior mean, variance, and the 95% confidence interval, is also derived from the retained 50,000 samples and given in Table 3. Similarly, the parameters of the Bayesian WAR model for peak acceleration are obtained in Fig. 5 and Table 3 after validation.

Fig. 6 illustrates the relationships of the RMS ( $\delta_{acc}$ ) and peak ( $P_{acc}$ ) acceleration responses versus 10-min wind speed ( $\bar{U}$ ) in logarithmic scale. It is evident that the increase in acceleration responses is in relation with the increase in mean wind speed. The estimated most plausible accelerations (red solid line) by the Bayesian approach match well with the measured responses, and the vast majority of the measurements lie, as expected, with the 95% predictive interval (red dashed lines).

By transferring the linear function form back to the power function expression, the corresponding parameters in the power regression models are obtained as listed in Table 4. Note that the coefficient  $b_2$  in the power regression model for peak acceleration is greater than  $b_1$  for RMS acceleration, which is consistent with the fact that the peak acceleration is larger than the RMS acceleration under the same wind speed. In order to investigate the performance of the formulated power regression models, R-squared ( $R^2$ ) is evaluated as a goodness-of-fit indicator. The R-squared is defined as [48]

$$R^2 = 1 - \frac{\sum_{i=1}^n (y_i - f_i)^2}{\sum_{i=1}^n (y_i - \bar{y})^2} \tag{18}$$

where  $y_i$  is the measured acceleration;  $f_i$  is the predicted acceleration by the regression models; and  $\bar{y}$  is the mean of the measured accelerations. The  $R^2$  ranges between 0 and 1. In the best case, the modeled values exactly match the observed values, which results in  $R^2 = 1$ . On the contrary, the model offers the worst predictions when  $R^2 = 0$ . The values of  $R^2$  for the two regression models are 0.891

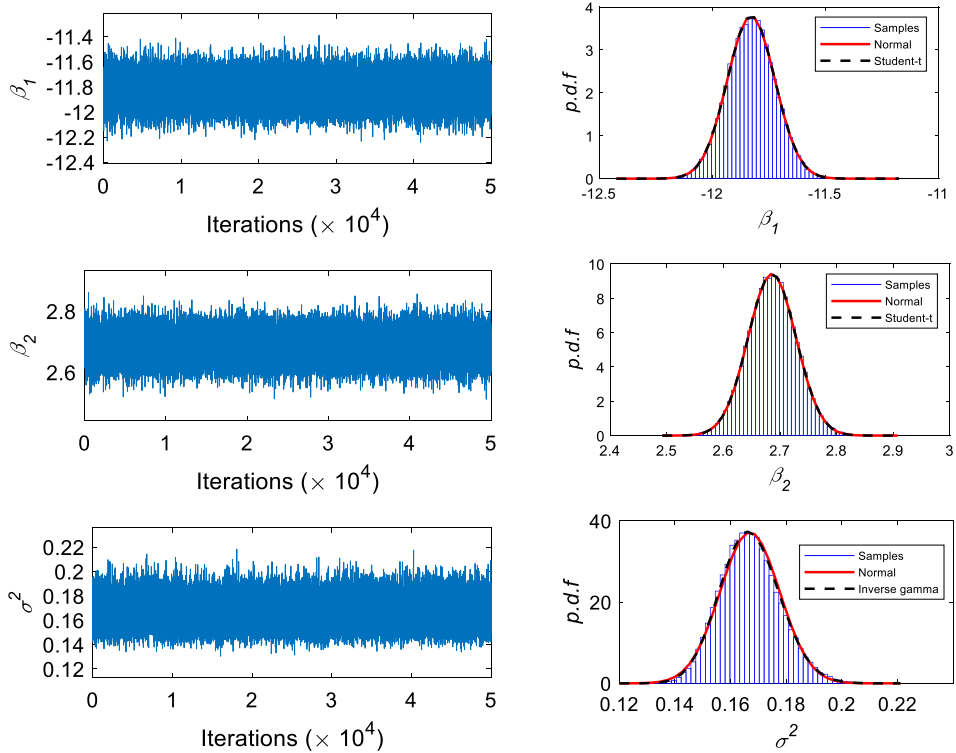


Fig. 5. Sample paths and estimated posterior densities for parameters (peak acceleration).

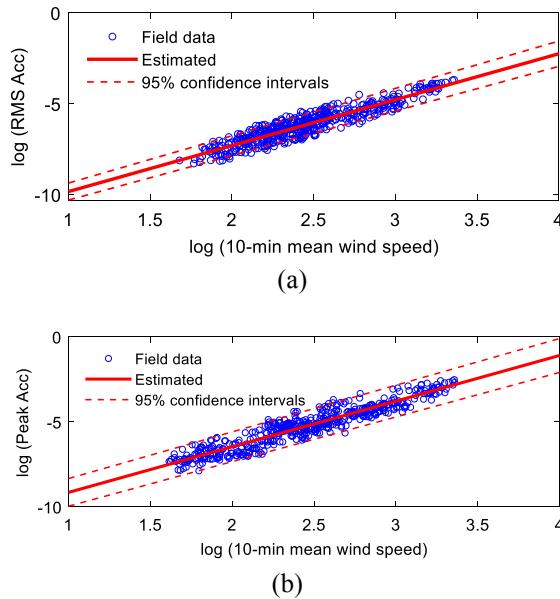


Fig. 6. Formulated Bayesian WAR models in logarithmic scale: (a) RMS acceleration; (b) Peak acceleration.

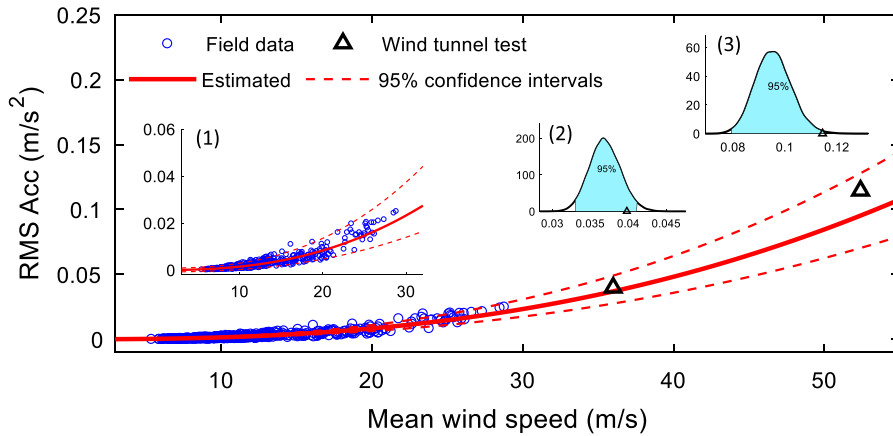
and 0.869, respectively, indicating that the formulated models perform favorably in prediction.

Fig. 7 illustrates the relationships between the RMS ( $\delta_{acc}$ ) and peak ( $P_{acc}$ ) acceleration responses and 10-min mean wind speed ( $\bar{U}$ ) in power function form. As shown in the figure, the estimated most plausible accelerations (red solid curves) with maximum probability match well with the measured responses, and the majority of the measurements lie within the 95% predictive interval except for some extrema.

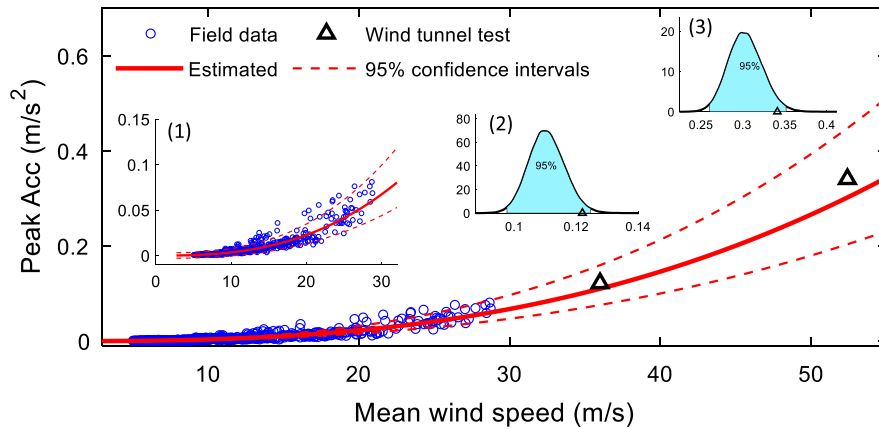
Since most of the measurement data are obtained at wind speeds below 30 m/s (Fig. 7a (1) and Fig. 7b (1)) during the 6 tropical

**Table 4**  
Parameters of regression models in Eqs. (16) and (17).

Model	Parameter	Mean	Standard deviation	95% confidence interval		R <sup>2</sup>
RMS	$a_1$	4.325E-6	0.504E-6	3.552E-6	5.201E-6	0.891
	$b_1$	2.527	0.046	2.437	2.619	
Peak	$a_2$	7.331E-6	0.775E-6	6.128E-6	8.888E-6	0.869
	$b_2$	2.686	0.042	2.603	2.769	



(a)



(b)

**Fig. 7.** Formulated Bayesian WAR models in power function form: (a) RMS acceleration: (1) view zoomed in measurement range, (2) predicted RMS acceleration under wind speed 36.7 m/s, (3) predicted RMS acceleration under wind speed 52.4 m/s; (b) Peak acceleration: (1) view zoomed in measurement range, (2) predicted peak acceleration under wind speed 36.7 m/s, (3) predicted peak acceleration under wind speed 52.4 m/s.

cyclones, field measurement data under high wind speeds (greater than 30 m/s) are not available to validate the predictive abilities of the formulated models in the case of strong wind conditions. Here, we instead use the wind tunnel test results to examine the prediction performance in extreme cases. The wind tunnel test of a scaled aeroelastic 3D model of the Canton Tower has been conducted in the TJ-2 Boundary Layer Wind Tunnel at Tongji University, China [49]. According to the wind tunnel test results, the maximum peak acceleration responses in all wind angles are 0.159 m/s<sup>2</sup> for 10-year return period (the wind speed atop the structure is 36.7 m/s) and 0.458 m/s<sup>2</sup> for 100-year return period (the wind speed atop the structure is 52.4 m/s), respectively. As the peak factor was set as  $g_f = 4$  in wind tunnel test, the corresponding maximum RMS acceleration responses in all wind angles can be calculated to be 0.040 m/s<sup>2</sup> for 10-year return period and 0.115 m/s<sup>2</sup> for 100-year return period, respectively. As shown in Fig. 7, the acceleration responses (marked with  $\Delta$ ) measured in wind tunnel test are slightly larger than the most plausible responses (red curves) estimated by the formulated

Bayesian WAR models in both 10-year return period (Fig. 7a (2) and Fig. 7b (2)) and 100-year return period (Fig. 7a (3) and Fig. 7b (3)) wind speeds, but they are within the 95% predictive interval. The reason for this difference may be due to the error of the scaled model used in the wind tunnel test or the error of the formulated prediction models. The proposed method is a data-driven approach, of which one drawback is its incapability to consider the difference in structural aerodynamics (e.g. aerodynamic damping) at low winds and high winds. Due to this difference, the Bayesian WAR models formulated using measurement data obtained under low winds may not fully represent the actual relationship between wind speed and wind-induced acceleration under high winds. However, the Bayesian WAR models can easily be updated with Bayes' theorem when new measurement data (especially those under wind speeds higher than 30 m/s) become available, enabling to generate evolutionary models for occupant comfort prediction of instrumented high-rise structures.

4.2. Comfort assessment by different criteria

A comparative study on the occupant comfort assessment of the monitored supertall structure during tropical cyclones is conducted herein by adopting four widely used comfort criteria, namely, ISO 6897 [12], ISO 10,137 [13], AIJ Guidelines [14], and Melbourne and Palmer's criterion [46]. Note that the ISO 6897 comfort criterion is based on RMS acceleration, while the other criteria are based on peak acceleration.

The ISO 6897 suggests using an RMS acceleration criterion with a 5-year return period for building structures. The RMS acceleration under wind actions with a 5-year return period should not exceed

$$\tilde{\delta}_{acc} = 0.026 \times f^{-0.412} \tag{19}$$

where  $\tilde{\delta}_{acc}$  is the RMS acceleration response of a structure; and  $f$  is the fundamental natural frequency (Hz) of the structure. A factor of 0.72 is used to convert the 5-year return period assessment curve into a 1-year return period curve.

The ISO 10,137 proposes two evaluation curves for 1-year return period: one for residences and the other for offices. It predicts a strong dependence of the peak acceleration upon the vibration frequency. The peak acceleration criterion for residences and offices is stipulated as:

$$\tilde{P}_{acc} = 0.04 \times f^{-0.445} \text{ for residences} \tag{20}$$

$$\tilde{P}_{acc} = 0.06 \times f^{-0.445} \text{ for offices} \tag{21}$$

Melbourne and Palmer [46] proposed a peak acceleration criterion for occupant comfort assessment with the following formula:

$$\tilde{P}_{acc} = \sqrt{2\ln(fT)} \left( 0.68 + \frac{\ln R}{5} \right) \exp(-3.65 - 0.41\ln f) \tag{22}$$

where  $f$  is the fundamental frequency of a structure;  $T$  is the time interval of segmented measurements in seconds;  $R$  is the return period in years; and the term  $\sqrt{2\ln(fT)}$  is essentially the gust factor for a normally distributed process. Hence, the RMS acceleration criterion

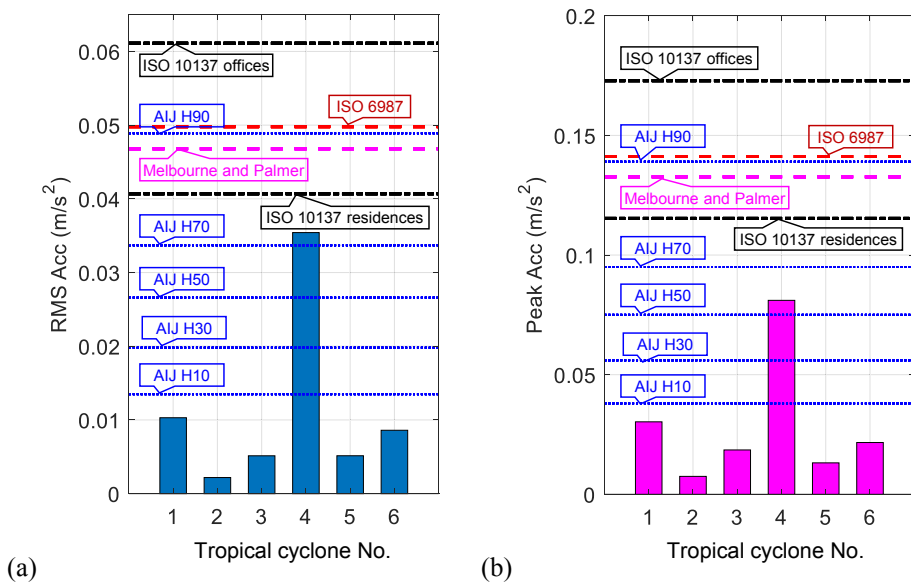


Fig. 8. Field-measured accelerations during 6 tropical cyclones against comfort criteria: (a) RMS acceleration; (b) Peak acceleration.

in line with Melbourne and Palmer’s peak acceleration can be deduced as

$$\tilde{\delta}_{acc} = \left(0.68 + \frac{\ln R}{5}\right) \exp(-3.65 - 0.41 \ln f) \tag{23}$$

The Architectural Institute of Japan Guidelines for evaluation of habitability building vibration provides five curves of motion perception, in which 10%, 30%, 50% 70% and 90% of people can perceive the vibration specified on each respective curve.

As aforementioned, the ISO 6897 criterion is stipulated in terms of RMS acceleration, while the other three criteria are based on peak acceleration. Hence, a conversion between the RMS acceleration and the peak acceleration should be made according to Eqs. (13) to (15) and by use of the gust factor  $\sqrt{2 \ln(fT)}$  proposed by Melbourne and Palmer [46].

Fig. 8 provides the maximum RMS and peak accelerations obtained from the measurement data during the 6 tropical cyclone events, and the comfort assessment results by the above four criteria after modulation to 1-year return period. The results show that both maximum RMS and peak accelerations during the tropical cyclones are all lower than the critical values suggested by the ISO 6897, ISO 10137, and Melbourne and Palmer’s criterion. The maximum RMS and peak accelerations generated during TC4 (Typhoon Vicente) merely exceed the H70 curve and H50 curve suggested by the AIJ Guidelines. It is concluded that the occupant comfort of the monitored supertall structure was satisfactory during the violent tropical cyclones between 2011 and 2013 according to the four widely used comfort criteria.

### 4.3. Probabilistic evaluation of occupant comfort

A noticeable feature of the Bayesian WAR models lies in that the predicted wind-induced acceleration given a wind speed is not a deterministic value, but rather a probability distribution. In practice, a primary concern is the probability of failure when a new set of measurements or predictions is available. For any structural component, the probability of failure is defined as the probability of violating a limit state. A limit-state function can be expressed as [38]

$$g(x) = R - S \tag{24}$$

where  $R$  is the resistance in terms of the maximum allowable acceleration stipulated in specifications,  $S$  is the measured/predicted acceleration during a strong wind, and  $g(x)$  is a performance function featuring the limit state of the structure in terms of acceleration. Failure occurs when the acceleration  $S$  exceeds the resistance  $R$  or when  $g(x) < 0$ . With the limit-state function, the probability of failure can be expressed as

$$P_f = P(g(x) < 0) = \int_{-\infty}^{\infty} F_R(x) f_S(x) dx \tag{25}$$

where  $F_R(x)$  is the cumulative distribution function (CDF) of the capacity and  $f_S(x)$  is the probability density function (PDF) of the measured/predicted acceleration. If  $R$  and  $S$  are independent Gaussian random variates with their mean values  $\mu_R$  and  $\mu_S$  and variances  $\sigma_R^2$  and  $\sigma_S^2$ , the failure probability can be determined as

$$P_f = \Phi\left(-\frac{\mu_R - \mu_S}{\sqrt{\sigma_R^2 + \sigma_S^2}}\right) \tag{26}$$

where  $\Phi(\cdot)$  is a standard normal probability function. The safety index is defined as

$$\lambda = -\Phi^{-1}(P_f) = \frac{\mu_R - \mu_S}{\sqrt{\sigma_R^2 + \sigma_S^2}} \tag{27}$$

where  $\Phi^{-1}(\cdot)$  is the inverse of the standard normal cumulative distribution function. The value of  $\lambda$  can be used to determine in a probabilistic manner whether the acceleration response  $S$  is within an acceptable range as compared to the resistance  $R$ . Obviously, a decrease of  $\lambda$  will result in a higher failure probability. For better quantifying the serviceability, the safety index  $\lambda$  is categorized into several ranges for assessing the significance of discrimination:  $\lambda < 0$  denotes ‘‘Complaints will occur’’;  $0 \leq \lambda < 1$  denotes ‘‘Complaints may occur’’,  $1 \leq \lambda < 2$  denotes ‘‘Perceptible but no complaints’’, and  $\lambda \geq 2$  denotes ‘‘Not perceptible in majority’’ [50].

To illustrate how the proposed method performs an alarm in ‘discomfort’ cases, the predicted accelerations at the wind speed 36.7 m/s (10-year return period) and 52.4 m/s (100-year return period) are considered as an example. The predicted distribution of the RMS acceleration at wind speed 52.4 m/s is first obtained by substituting the wind speed 52.4 m/s into the formulated Bayesian WAR model. Then the  $\mu_S$  and  $\sigma_S^2$  can be calculated based on the predicted probability distribution. As all the comfort assessment criteria stipulate only the maximum allowable acceleration values, the  $\mu_R$  is set as the maximum allowable acceleration while  $\sigma_R^2 = 0$ . The safety index characterizing comfort performance is then evaluated according to Eq. (27). As illustrated in Fig. 9, all safety indices (denoted with  $\diamond$  and  $\times$ ) in terms of RMS and peak accelerations at wind speed 52.4 m/s are far less than 0 (red dotted horizontal line), indicating that the predicted acceleration exceeds all comfort criteria suggested in the four guidelines, and occupant complaints will occur. In the case of wind speed 36.7 m/s, safety indices (denoted with  $\circ$  and  $*$ ) calculated according to the ISO 6897, ISO 10,137 for offices, Melbourne and Palmer’s criterion and AIJ H90 are larger than 2 (blue dotted horizontal line), implying that the vibration will not be perceived by occupants in majority, which satisfactorily meets the comfort criteria. Whereas safety indices derived from the AIJ

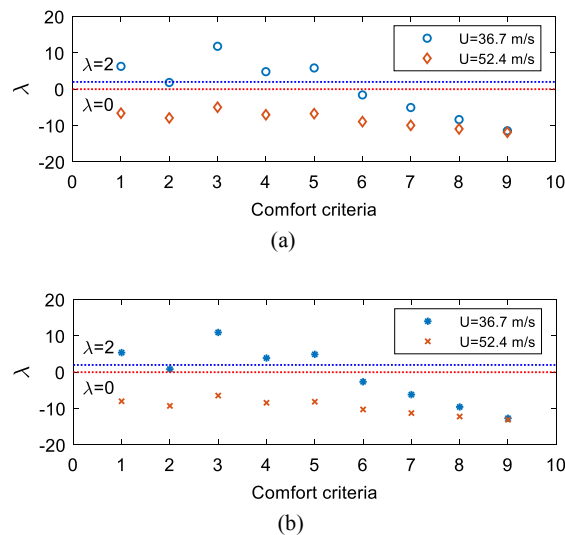


**Fig. 9.** Safety index for different comfort criteria: (a) RMS acceleration; (b) Peak acceleration (Note: The digits 1 through 9 denote the different comfort criteria: 1 – ISO 6897; 2 – ISO 10137 for residences; 3 – ISO 10137 for offices; 4 – Melbourne and Palmer’s criterion; 5 – AIJ H90; 6 – AIJ H70; 7 – AIJ H50; 8 – AIJ H30; 9 – AIJ H10).

H70, AIJ H50, AIJ H30 and AIJ H10 are less than 0, which do not meet the comfort criteria and will invoke occupant complaints. Safety indices calculated according to the ISO 10,137 for residences are between 1 and 2, that is, the vibration will be perceived by habitans but without complaint.

## 5. Conclusions

In this study, a probabilistic method in the context of Bayesian inference is proposed for the occupant comfort assessment of high-rise structures during tropical cyclones. In the formulated WAR model, the model parameters are treated as random variables with their distributions identified from monitoring data, and thus the model can explicitly account for uncertainties arising from measurement noise, environmental variability, and model error. By combining the formulated model and reliability theory, the elicited safety index provides a practical alternative to assess occupant comfort of wind-excited high-rise structures.

The proposed method has been verified by use of 186.8-hour field measurement data of wind effects on a 600 m high supertall structure during 6 tropical cyclones. The case study made the following observations: (i) The formulated Bayesian WAR models favorably characterize the correlation between the wind-induced acceleration response and wind speed, where uncertainties are duly reflected in the random model parameters and error parameters; (ii) The predicted acceleration responses by the Bayesian WAR models at 10-year and 100-year return periods wind speeds are a little less than the wind tunnel results; (iii) Occupant comfort evaluation results by four criteria in terms of RMS and peak accelerations indicate that the structural performance of the skyscraper was satisfactory over the three years of monitoring even during the violent tropical cyclones; (iv) The proposed safety index is capable of evaluating the probability of discomfort when the predicted acceleration distribution in regard to a future tropical cyclone is obtained. The larger the safety index, the higher the probability of comfort satisfaction for a high-rise structure.

## 6. Data availability statement

Some or all data, models, or code that support the findings of this study are available from the corresponding author upon reasonable request.

## Declaration of Competing Interest

The authors declare that they have no known competing financial interests or personal relationships that could have appeared to influence the work reported in this paper.

## Acknowledgements

The work described in this paper was supported by a grant from the Research Grants Council of the Hong Kong Special Administrative Region (SAR), China (Grant No. PolyU 152014/18E) and a grant from The Hong Kong Polytechnic University (Grant No. ZVR6). The authors would also like to appreciate the funding support by the Innovation and Technology Commission of the Hong Kong SAR Government (Grant No. K-BBY1).

## References

- [1] K.C. Kwok, P.A. Hitchcock, M.D. Burton, Perception of vibration and occupant comfort in wind-excited tall buildings, *J. Wind Eng. Ind. Aerodyn.* 97 (2009) 368–380, <https://doi.org/10.1016/j.jweia.2009.05.006>.
- [2] M.D. Burton, K.C. Kwok, P.A. Hitchcock, R.O. Denoon, Frequency dependence of human response to wind-induced building motion, *J. Struct. Eng.* 132 (2006) 296–303, [https://doi.org/10.1061/\(ASCE\)0733-9445\(2006\)132:2\(296\)](https://doi.org/10.1061/(ASCE)0733-9445(2006)132:2(296)).
- [3] Bashor R., Kareem A., Probabilistic performance evaluation of buildings: an occupant comfort perspective, Proceeding fo the 12th International Conference on Wind Engineering, Cairns, Australia, 2007.
- [4] BBC News, Typhoon Mangkhut: South China battered by deadly storm. <https://www.bbc.com/news/world-asia-45543664>, 2018 (accessed 13 July 2020.).
- [5] F.A. Johann, M.E. Carlos, F.L. Ricardo, Wind-induced motion on tall buildings: a comfort criteria overview, *J. Wind Eng. Ind. Aerodyn.* 142 (2015) 26–42, <https://doi.org/10.1016/j.jweia.2015.03.001>.
- [6] E. Bernardini, S.M. Spence, D.K. Kwon, A. Kareem, Performance-based design of high-rise buildings for occupant comfort, *J. Struct. Eng.* 141 (2015) 04014244, [https://doi.org/10.1061/\(ASCE\)ST.1943-541X.0001223](https://doi.org/10.1061/(ASCE)ST.1943-541X.0001223).
- [7] B.S. Taranath, *Structural analysis and design of tall buildings: steel and composite construction*, CRC Press, New York, USA, 2016.
- [8] R.O. Denoon, *Designing for wind-induced serviceability accelerations in buildings*, Ph.D. thesis, University of Queensland, 2000.
- [9] T. Kijewski-Correa, J. Kilpatrick, A. Kareem, D.K. Kwon, R. Bashor, M. Kochly, B.S. Yong, A. Abdelrazaq, J. Galsworthy, N. Isyumov, D. Morrish, R.C. Sinn, W. F. Baker, Validating wind-induced response of tall buildings: synopsis of the Chicago full-scale monitoring program, *J. Struct. Eng.* 132 (2006) 1509–1523, [https://doi.org/10.1061/\(ASCE\)0733-9445\(2006\)132:10\(1509\)](https://doi.org/10.1061/(ASCE)0733-9445(2006)132:10(1509)).
- [10] S. Lamb, K.C. Kwok, D. Walton, Occupant comfort in wind-excited tall buildings: motion sickness, compensatory behaviours and complaint, *J. Wind Eng. Ind. Aerodyn.* 119 (2013) 1–12, <https://doi.org/10.1016/j.jweia.2013.05.004>.
- [11] C. Pozzuoli, G. Bartoli, U. Peil, M. Globes, Serviceability wind risk assessment of tall buildings including aeroelastic effects, *J. Wind Eng. Ind. Aerodyn.* 123 (2013) 325–338, <https://doi.org/10.1016/j.jweia.2013.09.014>.
- [12] International Organization for Standardization (ISO), Guidelines for the evaluation of the response of occupants of fixed structures, especially buildings and offshore structures, to low-frequency horizontal motion (0.063 to 1 Hz) — ISO 6897, Geneva, Switzerland, 1984. <https://www.iso.org/standard/13419.html>.
- [13] International Organization for Standardization (ISO), Bases for design of structures – serviceability of buildings and walkways against vibrations — ISO 10137, Geneva, Switzerland, 2007. <https://www.iso.org/standard/37070.html>.
- [14] Architectural Institute of Japan (AIJ), Guidelines for the evaluation of habitability to building vibration, Japan, 2004.
- [15] M.D. Burton, K.C. Kwok, A. Abdelrazaq, Wind-induced motion of tall buildings: designing for occupant comfort, *Int. J. High-Rise Build.* 4 (2015) 1–8. <https://global.ctbuh.org/resources/papers/download/2311-wind-induced-motion-of-tall-buildings-designing-for-occupant-comfort.pdf>.
- [16] R.J. Hansen, J.W. Reed, E.H. Vanmarcke, Human response to wind-induced motion of buildings, *Journal of the Structural Division* 99 (1973) 1589–1605. <https://cedb.asce.org/CEDBsearch/record.jsp?dockey=0020329>.
- [17] T. Goto, Studies on wind-induced motion of tall buildings based on occupants’ reactions, *J. Wind Eng. Ind. Aerodyn.* 13 (1983) 241–252, [https://doi.org/10.1016/0167-6105\(83\)90145-9](https://doi.org/10.1016/0167-6105(83)90145-9).
- [18] B.E. Lee, The perception of the wind-induced vibration of a tall building: a personal viewpoint, *J. Wind Eng. Ind. Aerodyn.* 12 (1983) 379–384, [https://doi.org/10.1016/0167-6105\(83\)90059-4](https://doi.org/10.1016/0167-6105(83)90059-4).
- [19] Isyumov N., Kilpatrick J., Full-scale experience with wind-induced motions of tall buildings, Proceedings of 67th Regional Conference Council on Tall Buildings and Urban Habitat, Chicago, USA, 1996.
- [20] R.O. Denoon, C.W. Letchford, D.L. Morrison, Field measurements of human reaction to wind-induced building motion, in: *Wind Engineering Into the 21st Century* 1–3, 1999, pp. 637–644.
- [21] T. Kijewski-Correa, D.K. Kwon, A. Kareem, A. Bentz, Y. Guo, S. Bobby, A. Abdelrazaq, SmartSync: an integrated real-time structural health monitoring and structural identification system for tall buildings, *J. Struct. Eng.* 139 (2013) 1675–1687, [https://doi.org/10.1061/\(ASCE\)ST.1943-541X.0000560](https://doi.org/10.1061/(ASCE)ST.1943-541X.0000560).
- [22] Q.S. Li, J.Y. Fu, Y.Q. Xiao, Z.N. Li, Z.H. Ni, Z.N. Xie, M. Gu, Wind tunnel and full-scale study of wind effects on China’s tallest building, *Engineering Structures* 28 (2006) 1745–1758, <https://doi.org/10.1016/j.engstruct.2006.02.017>.
- [23] Q.S. Li, X. Li, Y. He, Monitoring wind characteristics and structural performance of a supertall building during a landfall typhoon, *J. Struct. Eng.* 142 (2016) 04016097, [https://doi.org/10.1061/\(ASCE\)ST.1943-541X.0001564](https://doi.org/10.1061/(ASCE)ST.1943-541X.0001564).
- [24] Q.S. Li, X. Li, Y. He, J. Yi, Observation of wind fields over different terrains and wind effects on a super-tall building during a severe typhoon and verification of wind tunnel predictions, *J. Wind Eng. Ind. Aerodyn.* 162 (2017) 73–84, <https://doi.org/10.1016/j.jweia.2017.01.008>.
- [25] X. Li, Q.S. Li, Monitoring structural performance of a supertall building during 14 tropical cyclones, *J. Struct. Eng.* 144 (2018) 04018176. <https://ascelibrary.org/doi/10.1061/%28ASCE%29ST.1943-541X.0002145>.
- [26] Y.L. Guo, A. Kareem, Y.Q. Ni, W.Y. Liao, Performance evaluation of Canton Tower under winds based on full-scale data, *J. Wind Eng. Ind. Aerodyn.* 104 (2012) 116–128. <https://www.sciencedirect.com/science/article/pii/S016761051200092X>.
- [27] Y.Q. Ni, K.C. Lin, L.J. Wu, Y.W. Wang, Visualized spatiotemporal data management system for lifecycle health monitoring of large-scale structures, *J. Aerosp. Eng.* 30 (2017) B4016007. <https://ascelibrary.org/doi/10.1061/%28ASCE%29AS.1943-5525.0000622>.
- [28] J.W. Zhang, Q.S. Li, Wind tunnel test and field measurement study of wind effects on a 600-m-high super-tall building, *Struct. Design Tall Spec. Build.* 26 (2017), e1385, <https://doi.org/10.1002/ta1.1385>.
- [29] D.M. Siringoringo, Y. Fujino, Wind-induced responses and dynamics characteristics of an asymmetrical base-isolated building observed during typhoons, *J. Wind Eng. Ind. Aerodyn.* 167 (2017) 183–197, <https://doi.org/10.1016/j.jweia.2017.04.020>.
- [30] X.G. Hua, K. Xu, Y.W. Wang, Q. Wen, Z.Q. Chen, Wind-induced responses and dynamic characteristics of a super-tall building under a typhoon event, *Smart Struct. Syst.* 25 (2020) 81–96, <https://doi.org/10.12989/sss.2020.25.1.081>.
- [31] L.C. Pagnini, G. Solari, Serviceability criteria for wind-induced acceleration and damping uncertainties, *J. Wind Eng. Ind. Aerodyn.* 74 (1998) 1067–1078, [https://doi.org/10.1016/S0167-6105\(98\)00098-1](https://doi.org/10.1016/S0167-6105(98)00098-1).
- [32] A. Pozos-Estrada, H.P. Hong, J.K. Galsworthy, Serviceability design factors for wind-sensitive structures, *Can. J. Civ. Eng.* 37 (2010) 728–738, <https://doi.org/10.1139/L10-013>.
- [33] D. Kong, J. Zhu, C. Duan, L. Lu, D. Chen, Bayesian linear regression for surface roughness prediction, *Mech. Syst. Sig. Process.* 142 (2020), 106770, <https://doi.org/10.1016/j.ymsp.2020.106770>.
- [34] Z.S. Ma, L. Li, Q. Ding, Multivariate recursive Bayesian linear regression and its applications to output-only identification of time-varying mechanical systems, *J. Vibration Cont.* (2020), <https://doi.org/10.1177/1077546320941703>.
- [35] M. Shin, J.S. Liu, Neuronized priors for Bayesian sparse linear regression, *J. Am. Stat. Assoc.* (2021), <https://doi.org/10.1080/01621459.2021.1876710>.
- [36] K.V. Yuen, *Bayesian methods for structural dynamics and civil engineering*, John Wiley & Sons, New York, USA, 2010.
- [37] Y.W. Wang, Y.Q. Ni, Bayesian dynamic forecasting of structural strain response using structural health monitoring data, *Struct. Control Health Monitor.* (2020), e2575, <https://doi.org/10.1002/stc.2575>.
- [38] Y.Q. Ni, Y.W. Wang, C. Zhang, A Bayesian approach for condition assessment and damage alarm of bridge expansion joints using long-term structural health monitoring data, *Eng. Struct.* 212 (2020) 110520, <https://doi.org/10.1016/j.engstruct.2020.110520>.
- [39] A.E. Gelfand, A.F. Smith, Sampling-based approaches to calculating marginal densities, *J. Am. Stat. Assoc.* 85 (1990) 398–409, <https://doi.org/10.1080/01621459.1990.10476213>.
- [40] Geweke J., Evaluating the accuracy of sampling-based approaches to the calculation of posterior moments, Federal Reserve Bank of Minneapolis, Research Department Staff Report No. 148, 1991.
- [41] G. Koop, *Bayesian Econometrics*, John Wiley & Sons, Chichester, United Kingdom, 2003.

- [42] Y.Q. Ni, Y. Xia, W.Y. Liao, J.M. Ko, Technology innovation in developing the structural health monitoring system for Guangzhou New TV Tower, *Struct. Control Health Monitor.* 16 (2009) 73–98, <https://doi.org/10.1002/stc.303>.
- [43] Y.Q. Ni, B. Li, K.H. Lam, D.P. Zhu, Y. Wang, J.P. Lynch, K.H. Law, In-construction vibration monitoring of a supertall structure using a long-range wireless sensing system, *Smart Struct. Syst.* 7 (2011) 83–102, <https://doi.org/10.12989/sss.2011.7.2.083>.
- [44] Y.Q. Ni, Y.W. Wang, W.Y. Liao, W.H. Chen, A vision-based system for long-distance remote monitoring of dynamic displacement: experimental verification on a supertall structure, *Smart Struct. Syst.* 24 (2019) 769–781, <https://doi.org/10.12989/sss.2019.24.6.769>.
- [45] D. Boggs, C.P. Petersen, Acceleration indexes for human comfort in tall buildings – peak or RMS, *Acceleration indexes for human comfort in tall buildings – peak or RMS*, CTBUH Monograph Chapter 13: motion perception tolerance and mitigation (1997).
- [46] W.H. Melbourne, T.R. Palmer, Accelerations and comfort criteria for buildings undergoing complex motions, *J. Wind Eng. Ind. Aerodyn.* 41 (1992) 105–116, [https://doi.org/10.1016/0167-6105\(92\)90398-T](https://doi.org/10.1016/0167-6105(92)90398-T).
- [47] T. Ando, *Bayesian Model Selection And Statistical Modeling*, CRC Press, Florida, USA, 2010.
- [48] A.C. Cameron, F.A. Windmeijer, An R-squared measure of goodness of fit for some common nonlinear regression models, *Journal of Econometrics* 77 (1997) 329–342, [https://doi.org/10.1016/S0304-4076\(96\)01818-0](https://doi.org/10.1016/S0304-4076(96)01818-0).
- [49] L.D. Zhu, Q.S. Ding, W. Chen, Wind tunnel test of aeroelastic full model of Guangzhou New TV Tower, Tongji University, Shanghai (in Chinese), 2006.
- [50] Y. Tamura, S. Kawana, O. Nakamura, J. Kanda, S. Nakata, Evaluation perception of wind-induced vibration in buildings, in: *Proceedings of the Institution of Civil Engineers — Structures and Buildings* 159, 2006, pp. 283–293, [10.1680/stbu.2006.159.5.283](https://doi.org/10.1680/stbu.2006.159.5.283).